Modeling of Crystallization in a Blend Containing at Least One Crystallizable Component: An Analogy from Eutectic Systems

Sudhakar Balijepalli[†] and Jerold M. Schultz*[,‡]

The Dow Chemical Company, 1702 Bldg., Corporate R&D, Midland, Michigan 48674, and Department of Materials Science, University of Delaware, Newark, Delaware 19716

Received January 13, 2006; Revised Manuscript Received June 28, 2006

ABSTRACT: It is shown that crystalline/crystalline and crystalline/noncrystalline blends can crystallize from the melt such that both components reside in the same spherulite. The observed morphology of such systems is that of growth arms of one component separated by regions rich in the other component. For crystalline/crystalline blends, cooperative crystallization is observed, such that the growth velocities of both species approach each other, allowing both components to crystallize nearly simultaneously. The crystallization and morphology of such systems are similar to those for eutectic crystallization of mixtures of small molecules. Existing analytical models describing the crystallization of eutectoid and eutectic systems of small molecules allow the growth velocity and the spacing of the alternating phases to be predicted. The model solves the moving boundary diffusion equation for the edgewise growth into the melt of a system of alternating plates of the two solid phases. Such a model has been adapted to the case of polymer blends. The problem is set up, and an analytical solution is found for low values of the Peclet number for crystallization $V\lambda/D_m$. It is found that the velocity of growth V is sharply peaked when plotted against the interarm spacing λ. Using measurements for a blend of high and low molecular weight poly(ethylene oxide)s, it is found that the operating condition for such growth corresponds to the maximum growth velocity. In the range of low Peclet numbers (low supercooling) reasonable agreement is found between measured and predicted values of both the growth velocity and the interarm spacing λ.

Introduction

It is frequently observed in blends of two polymers, of which one or both are crystallizable, that both components exist within a common spherulite. This is somewhat surprising since cocrystallization is rare, requiring that the two species separate into distinct domains within the spherulites. Particulary clear examples of the morphology for crystallizable/noncrystallizable blends can be seen in micrographs of spherulites in the poly(vinylidene fluoride)/poly(ethylene acrylate) system[1] and the syndiotactic/atactic polystyrene (PS) system.[2] Figure 1 shows melt-crystallized spherulites of a syndiotactic/atactic PS system from which the atactic material has been leached out. It is seen the spherulite is composed of growth arms of the syndiotactic species, separated from each other by domains of atactic material.

For crystallizable/crystallizable blends, one finds a similar morphology. Figure 2 shows an AFM amplitude image of the edge of a spherulite of a blend of high molecular weight poly(ethylene oxide) (PEO) and low molecular weight PEO.[3] Here the low molecular weight component has been selectively etched. The raised growth arms of the high molecular weight component are seen. These arms are separated by crystalline regions of the low molecular weight species.

For both cases, crystallizable/crystallizable and crystallizable/uncrystallizable blends, the morphology is that of alternating domains of chemically distinct materials. The morphology for at least one of the domains is that of growth arms, each growth arm consisting of a stack of crystalline lamellae separated by noncrystalline matter. The growth arm has the character itself of a plate or rod. In small molecule systems having a eutectic phase diagram (liquid → α(solid) + β(solid)), solidification from the melt is also in the form of alternating thin plates of α and β. This morphology forms in response to the need to redistribute species at the growth front; the redistributing species need move only small distances in the melt, from the front of one phase to

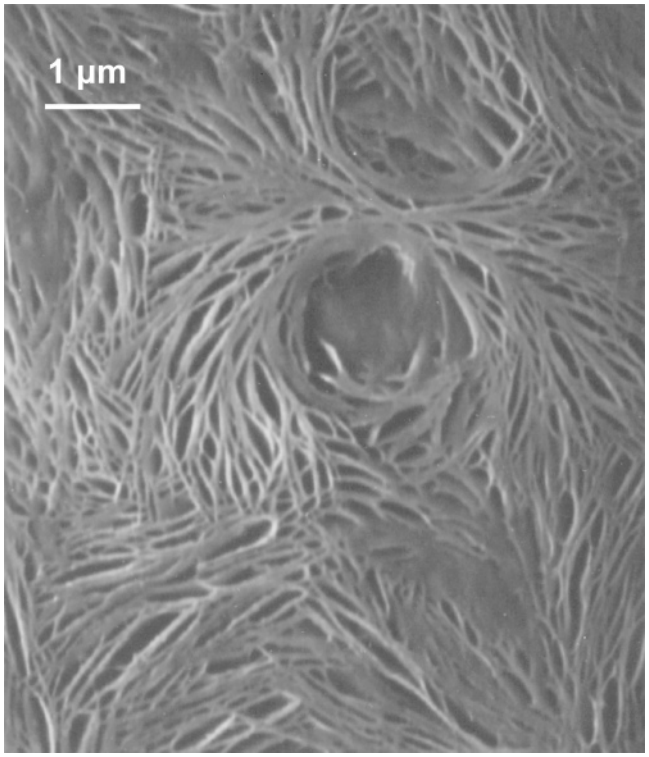

Figure 1. Scanning electron micrograph of a 50/50 blend of syndiotactic and atactic polystyrene which had been crystallized from the homogeneous melt at 240 °C. The atactic matrial has been dissolved out.

[†] The Dow Chemical Company.
[‡] University of Delaware.
* Corresponding author: e-mail schultz@che.udel.edu.

10.1021/ma060097v CCC: $33.50
Published on Web 09/20/2006

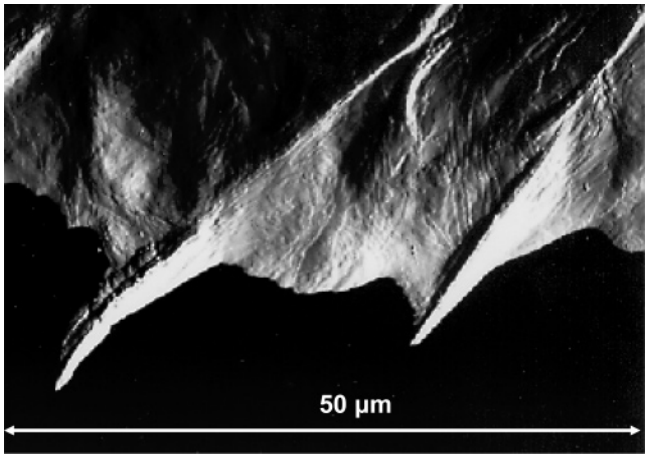

Figure 2. AFM height amplitude image of a 20/80 blend of high (270 000) and low (5000) molecular mass poly(ethylene oxide) crystallized from the melt at 54 °C. The low molecular mass material has been selectively etched away.

the front of the other. This diffusive motion is normal to the growth direction. This efficient redistribution process enables the rate of solidification to be maximized. For small molecule systems, reliable models and analyses are available to predict the growth velocity and the spacing of the substituent plates. The eutectic solidification situation is similar to the solidification of a crystallizable/crystallizable polymer, where again the constituents need to redistribute themselves at the growth front. Further, with only minor modification, the eutectic model can be adapted to the case of crystallizable/noncrystallizable polymers, in which the species present in the melt must redistribute themselves locally into alternating domains of growth arms of the crystallizable species and noncrystalline domains rich in the other species. (This situation is formally that of monotectic solidification, but the eutectic model is nonetheless analytically appropriate.)

In the case of crystalline/noncrystalline blends (or crystalline/crystalline blends solidifying above the melting point of one of the components[4]), the growth velocity of the crystallizing polymer is generally depressed below what it would be for the neat polymer. This is expected since the crystallizable component in the melt has been diluted by the noncrystallizable component and also because the mixing lowers the melting point and hence the undercooling. In the case of binary crystallizable/crystallizable blends solidifying below the melting point of both components, when the spherulite growth velocity has been measured, it is reported to be intermediate between the spherulite growth velocities of spherulites of each component in the unblended state. Such behavior has been observed in blends of (a) poly(ether ketone ketone) (PEKK) and poly(ether ether ketone) (PEEK),[5] (b) PEKKs with different isophthalate/terephthalate linkage ratios,[6] (c) nylon-6 and nylon-66,[7,8] and (d) poly(ethylene oxide)s of very different molecular weights.[9] The calorimetric fingerprint of this behavior is a combination of a single crystallization exotherm, or two closely spaced exotherms, in a temperature range different from what is expected for the neat polymers, and two melting endotherms, each at approximately the temperature expected for the neat polymer. An example of this behavior for a 50/50 blend of different PEKK copolymers is shown in Figure 3.[6] The kinetic manifestation is demonstrated in the overall crystallization rate and in the spherulite growth velocity. Figure 4 shows the crystallization half-time $\tau_{1/2}$ vs crystallization temperature for a 50/50 blend of PEEK and a PEKK copolymer.[5] Shown also

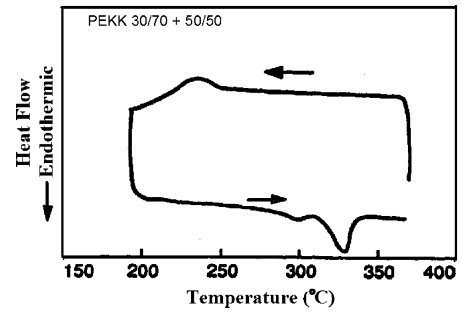

Figure 3. DSC cooling and heating scans of a 50/50 blend of different random copolymers of PEKK. The PEKK copolymers contain ratios of terephthalic to isophthalic linkages of 30 and 50%.

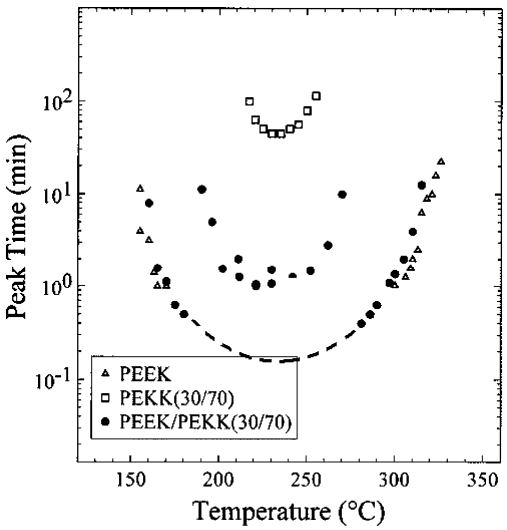

Figure 4. Plot of the time of the maximum in the DSC isothermal crystallization exotherm vs crystallization temperature for a 50/50 blend of PEEK and a random copolymer of PEKK (30% terephthalic linkage, 70% isophthalic linkage).

are curves representing the results for the neat polymers. For PEEK, crystallization over the central temperature range is too rapid to be measured. A dashed line indicates qualitatively how the results would appear over this range (consistent with the general behavior of polymer crystallization from the melt). We see in Figure 4 that over a range of temperatures, including the temperature of maximum crystallization rate (smallest $\tau_{1/2}$), the crystallization rate is much slower than that of the more rapidly crystallizing component and much faster than for the slower component in its neat state. (Outside this temperature range, only PEEK crystallizes; the growth velocity of the PEKK copolymer is too small to occur.) It is clear that there is some form of cooperation between the two components during crystallization; hence the term cooperative crystallization. (Cooperative crystallization, in which the two phases exhibit different melting points, is incompatible with a true (thermodynamic) eutectic, in which the phases must melt coherently. In the context of this paper, "eutectic modeling" refers to the kinetic modeling of two-phase system crystallizing from a one-phase melt.) This behavior can also be seen in the spherulite growth velocity.[5]

The lowering of the growth velocity of the faster crystallizing component is due to the exclusion of the unincorporable component and the buildup of its concentration in the melt adjacent to the growth surface. The growth velocity of the faster crystallizing material is to be predicted by the eutectic model,

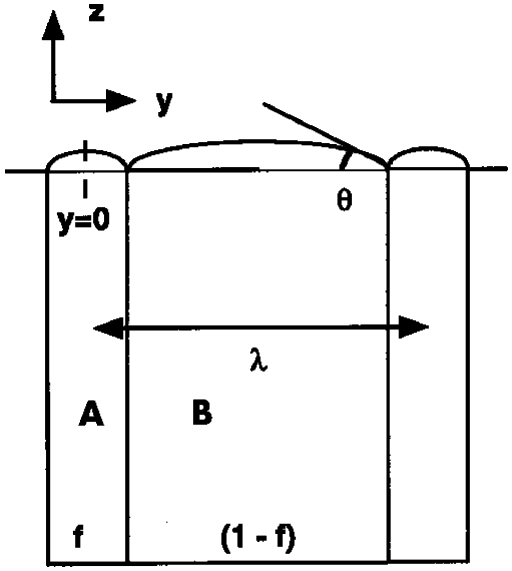

Figure 5. Schematic of eutectic model.

as is the growth arm spacing. For the slower crystallizing component in crystalline/crystalline blends, we as yet have no good model for how its growth velocity is enhanced, but that question need not be answered here.

Analysis: Steady-State Eutectic-like Growth

We consider here the simultaneous propagation of growth arms of two components from a homogeneous binary blend. The situation is sketched in Figure 5. Arms of components A and B grow cooperatively, with a periodicity λ and volume fractions f and $1 - f$. We may envision the arms as composed of edge-on crystal lamellae (the lamellae separated from each other by amorphous layers). The growth arms would then be thick in the x-direction, and we approximate this situation as a two-dimensional (yz) problem. As the growth front propagates forward, chains of component A must diffuse toward the component A arm front and away from the component B arm front (or from the noncrystalline material separating the growth arms, in the case of crystallizable/noncrystallizable blends) and conversely for component B.

The situation of Figure 5 is identical to that of a eutectic system growing from the melt and is similar also to eutectoid growth (γ(solid) $\rightarrow$ α(solid) + β(solid)). These transformations have been well studied in the metallurgical literature. The basis for the theoretical work was laid by Zener in 1946 for the iron−carbon eutectoid system.[10] Zener recognized that the most facile process is one whereby diffusion is predominantly normal to the growth direction, i.e., predominantly in the y-direction. The mean diffusion distance would then be approximately the periodicity of the system, and this would be arbitrarily small if interfacial energy were not created between the arms. The creation of interlamellar surfaces mediates against the reduction of λ. The net effect is that there will be some value of λ which optimizes some operating principle, such as maximum rate of free energy reduction or entropy production, the maximum linear growth velocity, or the maximum mass rate of transformation. Zener[6] proposed that growth occurs at the maximum linear velocity. Jackson and Hunt[11] and subsequent investigators[12−16]

There is no conceptual difference between the metallurgical models and the present case of cooperative growth in polymer blends. However, in the actual implementation of the Zener−Jackson−Hunt (ZJH) model, it is assumed that the process occurs close to equilibrium. This assumption is correct in the metallurgical case and provides a useful simplification to the analysis. Polymers, on the other hand, always crystallize at large undercoolings—i.e., far from equilibrium—and obey specific kinetics of attachment of molecules to the growth surface. Algebraically, these rules are usually associated with Lauritzen and Hoffman[17,18] (LH), although simpler models come to similar results. The result, in the LH format, is

$$V_0(T) = K_0 \exp\left[-\frac{U^*}{R(T - T_\infty)}\right] \exp\left(-\frac{K_g}{T(T - T^\circ_m)}\right) \quad (1)$$

where $V_0(T)$ is the linear growth velocity, K_0 is a constant, U^* is an activation energy for transport to the growth surface, R is the gas constant, T is the temperature of crystallization, T_∞ is the temperature at which chain mobility is effectively frozen, and T°_m is the equilibrium melting point of an infinitely large crystal. The second exponential term represents the driving force for crystallization, where K_g contains surface energies, the heat of fusion, ΔH_f, and the equilibrium melting point. The first exponential (the transport factor) is an increasing function with temperature, while the second exponential (the driving force factor) decreases steeply with temperature, to become zero at the equilibrium melting point. While the result is a bell-shaped curve of growth velocity vs temperature, growth from the melt most often occurs on the high-temperature decline of the curve.

It should be noted that other simplified kinetic growth rate expressions would have been adequate for the sake of modeling. However, the steep changes in growth rate and the attendant changes in morphology with temperature of crystallization for polymers are better served by the LH model.

In real cases the growth morphology is that of growth arms propagating into the melt. The interface between the growth arm and the melt provides a capillarity effect which lowers the melting point below its equilibrium value. Let this value of the melting point be T^*_m. The Gibbs−Thompson for this situation can be written

$$\Delta T^\circ_m = T^\circ_m - T^*_m = \Gamma_R \kappa \quad (2)$$

where κ is the local curvature of the interface and

$$\Gamma_R = \frac{2\sigma T^\circ_m}{\Delta h_f} \quad (3)$$

where σ is the solid-melt surface energy. The average curvature for the situation of Figure 5 is[14]

$$\kappa = \frac{2 \sin \theta}{f\lambda} \quad (4)$$

and the equilibrium melting point, adjusted for capillarity, is

$$T^*_m = T^\circ_m - \frac{2\Gamma_R \sin \theta}{f\lambda} \quad (5)$$

The melting point can also be decreased by the concentration of the melt at its interface with the growing A or B crystals. In the general case this must be considered. The equilibrium melting point corrected for the presence of a solutal species is

$$T_m = T^*_m - m c_B^{int} \quad (6)$$

where m is the slope of the liquidus curve (assumed to be a straight line) and c_B^{int} is the local concentration of the solutal species at the interface at steady state.

It is convenient to rewrite (1) as

$$V_0(\kappa,T,c_B^{int}) = K_0 \exp\left[-\frac{U^*}{R(T-T_\infty)}\right]\exp\left(-\frac{K_g}{T(T-T_m)}\right) \quad (7)$$

In the present work, we will test the theoretical results by comparison with experiments on high/low molecular weight PEO blends. In this case, a value of 1.0×10^{-6} cm·K is used for $2\Gamma_R \sin\theta$ in (5), consistent with usage in a previous publication.[19]

In the case described in Figure 5, the velocity $V(T)$ is lower than $V_0(T)$ because of concentration and capillarity effects specific to the alternating lamellae morphology. Here the growth velocity $V(T)$ includes a dilution effect and can be expressed as a Taylor's expansion about small curvature and compositional changes:

$$V = V_0(\kappa_0,T,c_B^\infty)(1-c_B^{int})[1+\beta_1(\kappa-\kappa_0)+\beta_2(c_B^{int}-c_B^\infty)] \quad (8)$$

where (again) κ and κ_0 are the actual interface curvature and the equilibrium interface curvature and β_1 and β_2 are Taylor's coefficients. In (8) the $1-c_B^{int}$ term accounts for the dilution of component A in front of the growing A-arm crystal. It is expected that in most cases this will be the dominant term. There is no reason to expect that κ will be significantly different from κ_0, and for systems in which the A and B chains are similar (and the interaction parameter χ_{AB} small) β_2 will be small. As a reasonable approximation, we write then for the propagation of the A-arm

$$V \cong V_0(\kappa,T,c_B^\infty)(1-c_B^{int}) \quad (9)$$

Henceforth, the expression $V_0(\kappa,T,c_B^\infty)$ is written as $V_0(\lambda,m,T)$ representing the kinetic growth rate expression corrected for curvature and solutal undercooling. Averaging over the growth surface, we have

$$\frac{2}{f\lambda}\int_0^{f\lambda/2} V\,dy = \frac{2V_0(\lambda,T)}{f\lambda}\int_0^{f\lambda/2}(1-c_B^{int})\,dy = \frac{2V_0(\lambda,T)}{f\lambda}(1-\bar{c}_B^{int})$$

or

$$V = V_0(\lambda,m,T)(1-\bar{c}_B^{int}) \quad (10)$$

where the overbar indicates the mean value. Equation 10 represents the operating equation of the growing system. The steady-state velocity V is simply the kinetic growth velocity altered by the concentration of species B at the interface, which in turn is decided by diffusion of the species, the kinetic growth velocity, and the spacing λ. The rest of the exercise is to determine $\bar{c}_B^{int}$ from the coupled diffusion-kinetic problem at the interface.

The core of the present work is to describe the growth of the periodically alternating component A/component B lamellar front into the melt. During the propagation of the front, component B is rejected from A-lamellae and component A is rejected from B-lamellae. For steady-state growth (as is usually observed) the diffusion equation for component B is

$$\frac{\partial^2 c_B}{\partial y^2} + \frac{\partial^2 c_B}{\partial z^2} + \frac{V}{D_m}\frac{\partial c_B}{\partial z} = 0 \quad (11)$$

where c_B is the fraction of component B in the melt and D_m is the diffusivity of component B in the melt. In the following analysis, the variation of D_m with melt composition is assumed to be negligible. The boundary conditions describing the periodic field in front of lamellae of component A are

$$\text{periodicity:}\quad c_B(y+\lambda) = c_B(y)$$

$$\text{symmetry:}\quad \frac{\partial c_B}{\partial y} = 0 \text{ at } y = 0,\ y = \lambda/2$$

$$\text{far field:}\quad c_B = c_B^\infty \quad (12)$$

where c_B^∞ is the original composition of B in the melt.

The most general composition profile satisfying (11) and (12) is

$$c_B = c_B^\infty + A\exp\left(-\frac{Vz}{D_m}\right) + \sum_{i=1}^{n} B_n \exp(-b_n z)\cos\left(\frac{2n\pi}{\lambda}y\right) \quad (13)$$

where A, B_n, and b_n are constants to be determined using the boundary conditions.

Substituting (13) into (11), b_n is found to be

$$b_n = \frac{Pe + \sqrt{(2\pi n)^2 + Pe^2}}{\lambda} \quad (14)$$

where Pe is the Peclet number for growth of this eutectic-like system and is defined as

$$Pe = \frac{V\lambda}{D_m} \quad (15)$$

It is to be noted that D_m/V is the diffusion length δ, a measure of the distance an average molecule diffuses during the process. Roughly then, this Peclet number is the ratio of the diffusive distance required (one-half the lateral period) to the distance an average chain diffuses. For Pe significantly less than 1, $\delta \gg \lambda$ and the composition fields of adjacent growing arms overlap. The system should then readjust its morphology, to increase λ, thereby affording a greater growth velocity. For Pe significantly greater than 1, the diffusion distance becomes much smaller than the growth arm spacing and the arms grow independently of each other. The interest here is in the $Pe < 1$ regime. For small Peclet numbers (the case to be examined here), $2n\pi \gg Pe$, and $b_1 = 2\pi/\lambda$.

We now determine the other constants, B_n and A. B_n is found using the mass conservation conditions at the growth front:

$$\left(\frac{\partial c_B}{\partial z}\right)_{z=0} = \frac{V}{D_m}c_B^{int}, \quad \text{for } 0 \le y \le \frac{f\lambda}{2} \quad (16)$$

$$\left(\frac{\partial c_B}{\partial z}\right)_{z=0} = \frac{V}{D_m}(1-c_B^{int}), \quad \text{for } \frac{f\lambda}{2} \le y \le \lambda \quad (17)$$

where c_B^{int} is the concentration of B at the interface. We multiply both sides of eqs 16 and 17 by $\cos[(2m\pi/\lambda)y]$ and then integrate the sum of (16) and (17) from 0 to $\lambda/2$. This leads to

$$B_n = \frac{2}{n\pi}\frac{V}{D_m}\frac{\sin(n\pi f)}{\left(b_n - \frac{V}{D_m}\right)} \tag{18}$$

The constant A is found in the following way. First a mass conservation equation, averaged over the interface, is written

$$\int_0^{f\lambda/2} c_B^{int} V\,dy = -D_m \int_0^{f\lambda/2}\left(\frac{\partial c_B}{\partial z}\right)_{c_B = c_B^{int}} dy \tag{19}$$

We now substitute the composition profile (13) and the growth velocity expression (10) into (19). In eq 13 for the composition we find the sum $\sum_{i=1}^{n} B_n \exp(-b_n z)\cos[(2n\pi/\lambda)y]$. This is required on the left of (19) and its derivative with z, $-\sum_{i=1}^{n} b_n B_n \exp(-b_n z)\cos[(2n\pi/\lambda)y]$, is needed on the right. Seeking an analytical solution, we restrict ourselves to consideration of low Peclet numbers only. For this case, the terms of the summations above quickly vanish for $n > 1$, and we may then consider integrating only the leading terms, giving

$$\sum_{i=1}^{n} B_n \exp(-b_n z)\cos\left(\frac{2n\pi}{\lambda}y\right) \approx 2Pe\,\frac{\sin^2(\pi f)}{(\pi)^3 f} \tag{20}$$

and

$$\sum_{i=1}^{n} b_n B_n \exp(-b_n z)\cos\left(\frac{2n\pi}{\lambda}y\right) \approx 2\frac{V}{D_m}\frac{\sin^2(\pi f)}{\pi^2 f} \tag{21}$$

Using these simplifications in (19), we carry out the integrations, ignoring small terms in powers greater than 1 of the Peclet number. Solving for A, we have

$$2(c_B^{\infty} + A) = \left\{\left[\left(\frac{V}{V_0} - 1\right) + \frac{2Pe}{\lambda}F_1(\lambda f)\right]^2 + 4\left[\left(\frac{V}{V_0}c_B^{\infty} + F_1(\lambda f)\right)\left(\frac{Pe}{\lambda} - 2\frac{V}{V_0}\right)\right]\right\}^{1/2} - \left[\left(\frac{V}{V_0} - 1\right) + \frac{2Pe}{\lambda}F_1(\lambda f)\right] \tag{22}$$

where

$$F_1 = \frac{\sin^2(\pi f)}{\pi^2 f} \tag{23}$$

Having expressions for B_n, b_n, and A, the interface concentration $\bar{c}_B^{int}$ is now fully determined by the interface velocity V and the periodicity λ. Equation 10 can now be used as the operating equation to establish V as a function of λ. Using the definition of the Peclet number for growth (15) in (10), the operating equation is now

$$\frac{Pe}{Pe_0} = 1 - \bar{c}_B^{int}(Pe, Pe_0) \tag{24}$$

where

$$Pe_0 = \frac{V_0(\lambda,m,T)\lambda}{D_m} \tag{25}$$

Here $V_0(\lambda,m,T)$ is the growth velocity of the neat polymer, but reflecting also the effects of periodicity λ and the solutal undercooling m on the melting point.

One proceeds to solve (24) in the following way. For a given temperature T, $V_0(T)$ for the neat polymer is found from experimental growth velocities, assuming a flat front with $\lambda = \infty$. The velocities are corrected for curvature and solutal undercooling to obtain $V_0(\lambda,m,T)$. For a chosen λ, eq 24 is iterated until a fit is found for Pe. Using $V(\lambda,m,T) = (D_m/\lambda)Pe$, the growth velocity $V(\lambda,m,T)$ is then found, using experimental or theoretically estimated values of the diffusivity D_m.

Experiment

To test the eutectic model solution, we have used blends of high (270 000) and low molecular (5000) mass poly(ethylene oxide)s (PEOs). The materials and some of the crystallization behavior of the blends were described previously.[9] To test the analysis, one needs values of the growth velocity V, the interarm spacing λ, and the diffusivity D_m. Furthermore, the values of $V_0(T)$ for the neat polymer, the associated LH parameters and the slope of solutal undercooling m, are also required.

Materials and Blends. PEO fractions, $M_w \sim 270\,000$ ($M_w/M_n \sim 1.1$) and $M_w \sim 5000$ ($M_w/M_n \sim 1.05$), were obtained from Pressure Chemical Co. and Polysciences Inc., respectively. Blends of PEO fractions were prepared by dissolving the two components in benzene and solution casting them in a nonsolvent, isooctane. The resulting powders were dried in a vacuum for a week. Powders of the blends were melted to prepare appropriate samples for measurement.

Optical Microscopy. Optical microscopy studies were carried out with a Nikon Microphot-SA microscope in conjunction with a Mettler hot stage (FP-82). Powders of the sample weighing ~5−7 mg were melted on glass slides to form thin films ~20−50 μm thick. The specimens were heated to 90 °C to melt the film and were then quickly inserted into the hot stage set at a prefixed crystallization temperature. The hot stage was caliberated with a melting point standard, and the temperature control was ±0.2 K. Seven temperatures between 42 and 56 °C were used. The growth of spherulites was recorded on a VCR, and an image analysis program was used to extract growth rate data from time-lapsed frames of spherulitic fronts. Polarized light and Hoffman modulation contrast were employed to observe the morphology.

The following data were obtained: $V_0(T)$ for the neat high molecular weight fraction and $V(\lambda,T)$ for the blend. The growth rate for the neat polymer was fitted to the LH model to obtain $K_g = 7.37 \times 10^4$ K^2 and the preexponential factor $K_0 = 9.3 \times 10^{11}$ cm/s. Other parameters in the kinetic expression are as follows: $T_\infty = T_g - 30$ K where T_g of PEO is 206 K. The quantity $U^* \sim 29.3$ kJ/mol was taken from the work of Kovacs.[20]

Differential Scanning Calorimetry. Differential scanning calorimetry was carried out on the neat and blend samples using a Perkin-Elmer DSC7 system. Typical sample weights were 6−8 mg. Samples were melted to a temperature of 90 °C and quenched to an isothermal crystallization temperature. The exothermic crystallization processes was followed by monitoring the melting endotherm at a heating rate of 20 °C/min. The melting temperatures (taken from the maximum in the endotherm) were corrected for heating rate. The high molecular weight component is reported to have a $T_m^\circ = 343.2$ K. The depression in melting point of the blend systems were also measured by the same technique, and the reported slope of the liquidus line as a function of concentration of the solutal species is $m = 5.2$ K/(mol/mol).

Atomic Force Microscopy. Thin films of blend samples were crystallized isothermally on a glass slide. The samples were subsequently etched in a solvent mixture of 20% benzene and 80% isooctane for 2 min in an ultrasound bath. As a result, the low molecular weight component was preferentially etched out, and the morphology of bundles of the high molecular weight component was left behind for study. Samples were dried and mounted on stainless steel disks for atomic force microscopy.

Atomic force microscopy experiments were carried out using a Digital Instruments Nanoscope III Multimode scanning probe. The tapping mode of operation was employed to image sample surfaces. Single-crystal silicon tips having a nominal force constant of 0.064 N/m and a cantilever with a resonance frequency between 100 and 600 kHz were used.

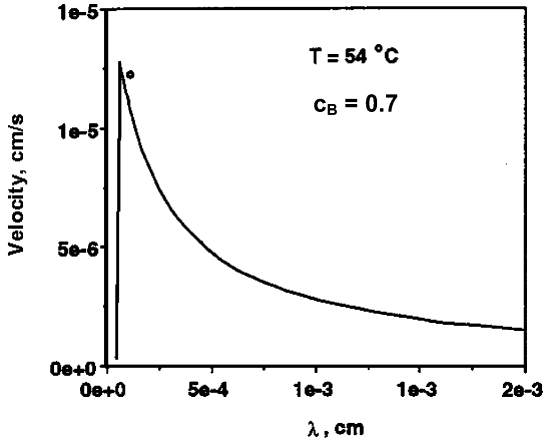

Figure 6. Computed growth velocity vs growth arm spacing for a 30/70 blend of high and low molecular weight poly(ethylene oxide). Observed operating point also shown.

A total of 12 independent measurements averaging three scans were used to calculate the mean values of bundle spacing (λ). With the concept in mind that growth arms are spawned near each other and then diverge, we take the minimum spacing between neighboring pairs of growth arms to represent λ; this is the spacing at which the growth arms are likely to be at their maximal velocity.

Mutual Diffusion Coefficient. D_m is computed from literature values for the diffusivities of neat PEOs. In determining the value of D_m, we begin with an expression for short chains (B) diffusing through long chains (A), with both species beyond the entanglement limit:[21]

$$D_m = c_A D_B + c_B D_A \tag{26}$$

Here the intrinsic diffusion coefficients D_B and D_A are given by

$$D_A = N_A D_A^* \left[\frac{c_B}{N_A} + \frac{c_A}{N_B}\right]$$

$$D_B = N_B D_B^* \left[\frac{c_B}{N_A} + \frac{c_A}{N_B}\right] \tag{27}$$

where N_B and N_A are the number of monomer units in the two chain species, N_e is the entanglement degree of polymerization, and D_A^* and D_B^* are the self-diffusion coefficients for the two species. Based on the reported entanglement molecular weight of 4400,[20] $N_e = 100$. For the PEO polymers used here, the self-diffusivities of the short chain species[22] and the long chain species[23] are given respectively by

$$D_A^* = 6.65 \times 10^{-5} \exp\left(-\frac{23\,000}{RT}\right) \quad \text{cm}^2/\text{s}$$

$$D_B^* = 1.03 \times 10^{-9} \exp\left(-\frac{16\,000}{RT}\right) \quad \text{cm}^2/\text{s} \tag{28}$$

The activation energy for D_B^* is extrapolated from values in the literature.[23]

Comparison of Prediction and Experiment

From the procedure outlined above for solving (24), one example result, for a 30/70 high/low molecular weight PEO blend crystallizing at 54 °C, is shown as Figure 6. We see here that the analytical solution for $V(\lambda,m,T)$ as a function of λ is sharply peaked. Shown also in Figure 6 is the observed operating point for this blend and temperature. The observed operating point (V^*,λ^*) is very close to the maximum in the curve. This is the typical result for small Peclet numbers. Selection based on the most rapid transformation is not unreasonable to expect,

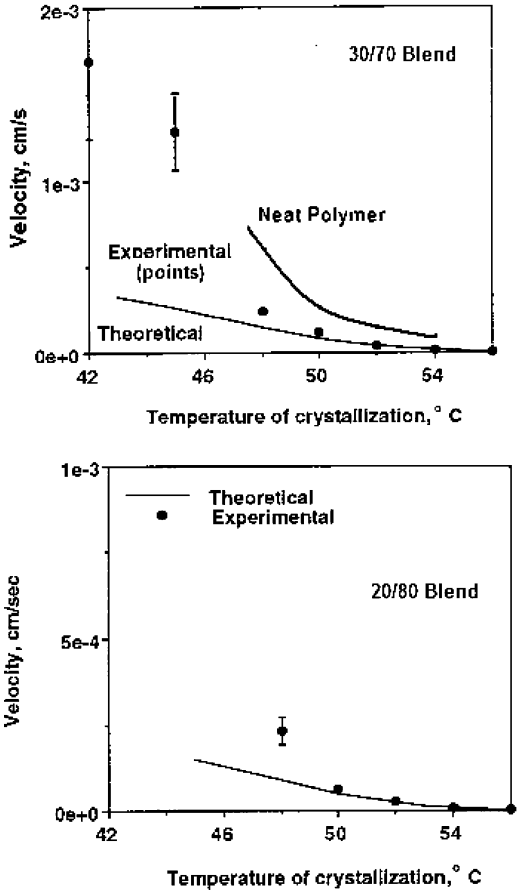

Figure 7. Computed and measured growth velocity vs crystallization temperature for 30/70 (above) and 20/80 (below) high/low molecular weight poly(ethylene oxide) blends.

and we therefore propose that the periodicity λ selected is that which maximizes the velocity of growth. This hypothesis aligns with that used by Zener and other early investigators in the study of eutectoid crystallization.[6]

The temperature used for Figure 6, 54 °C, corresponds to a very low Peclet number. The correspondence of observed operating point with the maximum in the analytical curve is good throughout the low *Pe* range but is progressively lost as *Pe* becomes larger. This is seen in Figure 7, which is a plot of the analytically derived operating point velocity vs crystallization temperature. Here, low values of *Pe* correspond to high temperatures, and the fit is quite good in that range.

A comparison of measured and analytically derived arm spacings λ vs crystallization temperature is shown in Figure 8. At the highest crystallization temperatures the measured arm spacing is about a factor of 2 higher than the predicted, not an unreasonable fit for an ab initio analysis. The absolute fit becomes poorer as the crystallization temperature is decreased, although the measured and analytical results show similar temperature dependence.

Discussion

The analysis given here applies to the case of crystalline/crystalline polymers which crystallize cooperatively (i.e., crystallizing approximately simultaneously, with a common front). In this case, the composition of the material between the somewhat faster growing arms is fixed simply as the somewhat slower growing material. The expectations from the model are as follows. The steady-state spacing and velocity of growth morphology of this two-phase transformation can be character-

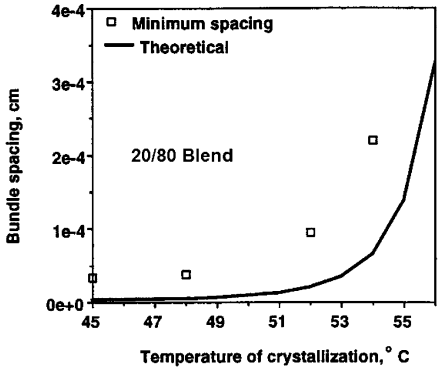

Figure 8. Computed and measured growth arm spacings vs crystallization temperature for a 20/80 high/low molecular weight poly(ethylene oxide) blend.

ized and captured by the analysis. As the growth arms approach each other, the proximity of the two phases results in an overlap in the concentration fields (of the noncrystallizing component). Decreasing λ still farther causes even greater overlap, and the increasing concentration at the interface reduces the growth velocity. On the other hand, as the spacing increases, the velocity adopted by the system becomes larger. However, these increasingly high growth rates as λ is increased lead to increased solute buildup and the growth velocity decreases. These competing processes lead to the maximum in the V vs λ plot. The operating point that seems to fit the data in this report is the maximum velocity of transformation. It should be mentioned that the capillarity effect described earlier does not strongly affect the results here, as shown by varying Γ widely in the computations (see below) and observing little change in the results.

The spacing at maximum velocity predicted by the model also fits reasonably well with experimental results. However, it should be noted that, experimentally, the high molecular weight component bundles show a large variation in spacing from a minimum spacing in the submicrons to a maximum spacing of several tens of microns. The large variation in spacing is a result of frequent branching of the lamellar bundles. Because of branching, the minimum spacing that is allowable is limited by the capillarity effect of bringing two phases into close proximity. A bound for the minimum spacing is then provided by the extremum operating point of the eutectic-like structure.

The analysis holds well at low velocities of growth as the two components have sufficient time to diffuse to their individual phases. At higher velocities or larger Peclet numbers, the experimental results for velocities are somewhat higher than the model predictions. A thorough examination of this situation has been carried out for the PEO blend system, and it was shown that at higher Peclet numbers the two phases do not grow individually as assumed by the model but that an element of cocrystallization of the two phases occurs.[9] In other words, there is some B in the crystal of A and vice versa. This kinetic incorporation of the components would require a modification of the existing model. But, conceptually, since the components in this scenario do not have diffuse far, the situation is less diffusion limited and would result in higher growth velocities.

The analysis should apply as well to crystalline/noncrystalline systems, but the operating condition may be altered. For crystalline/noncrystalline systems, the composition of the region separating growth arms is variable; its concentration of crystallizable material is not fixed and can change to enhance the rate of transformation. This situation applies also to the stacking of crystalline lamella, separated by noncrystalline matter, within the growth arms. One can imagine in this case that the most rapid growth of the crystal lamellae would occur at very large spacings between the lamellae, since then the noncrystalline species excluded by each lamella would not interfere with the growth of its neighbors. But for this condition to exist, the noncrystalline layers would contain massive amounts of the crystallizable component, and the mass transformed would be very small. A finite element model of this situation[24] suggested that the operating condition should be the maximum rate of mass transformation, which is the maximum of the product of growth velocity and crystalline fraction within the stack. Quite likely this operating condition should also apply to the growth arm behavior in crystalline/noncrystalline blends.

Finally, it should be mentioned that in the analysis above the shape of the interface had been treated in two different ways. For the capillarity effect on the melting point, the interface was taken to be curved. But in the application of the boundary conditions in the solution to the diffusion equation, the interface was taken to be everywhere at $z = 0$; i.e., the interface was taken as being flat. This latter assumption was made in the interest of mathematical expediency, while the capillarity effect of the curved interface was left (a) to approximate reality and (b) to indicate how that portion of the melting point decrement could be handled. To examine the severity of the mistreatment of the interface shape, a sensitivity test was made. It was found that a 5-fold increase in the capillarity parameter Γ produced no discernible change in the results.

Summary

When polymer crystalline/noncrystalline or crystalline/crystalline blends crystallize from the melt, they can do so by a mechanism in which both components appear within the same spherulite. Here the growth arms of one polymer species are separated by regions rich in the other species. For crystalline/crystalline polymers the mechanism is cooperative crystallization, in which adjacent arms are of different species. In the present work, an analytical model of eutectic solidification for small molecule systems has been adapted for use in predicting the growth velocity and interarm spacing of such systems. A chief difference between the small-molecule and the polymer models is the incorporation of a strongly temperature-dependent crystallization velocity in the latter case. Because of assumptions made in the analysis, the analytical solution should be valid only for low Peclet crystallization numbers $V\lambda/D_m$. A blend of poly(ethylene oxide)s of 270 000 and 5000 molar mass was studied experimentally. The correspondence of measured and computed growth arm spacings and growth velocities is good in the low Peclet number (low supercooling) region.

Acknowledgment. This work was supported by the National Science Foundation under Grant DMR-9115308.

References and Notes

(1) Briber, R. M.; Khoury, F. *Polymer* **1987**, *28*, 38.
(2) Kit, K. M.; Schultz, J. M. *J. Polym. Sci., Polym. Phys. Ed.* **1998**, *36*, 873−888.
(3) Balijepalli, S. PhD Dissertation, University of Delaware, 1996.
(4) Penning, J. P.; John Manley, R. St. *Macromolecules* **1996**, *29*, 84−90.
(5) Wang, W.; Schultz, J. M.; Hsiao, B. S. *Proc. NRC−CNRC Composites '96 and Oriented Polymers Symp., Oct. 9−11, Boucherville, QC, Canada* **1996**, 452−460.
(6) Hsiao, B. S.; Gardner, K. H.; Schultz, J. M.; Wang, W. *Proc. Soc. Plastic Engineers Meeting, ANTEC '93, New Orleans, May 9−13* **1993**, 1004−1009.
(7) Evstatiev, M.; Schultz, J. M.; Petrovich, S.; Georgiev, G.; Fakirov, S.; Friedrich, K. *J. Appl. Polym. Sci.* **1998**, *67*, 723−737.

(8) Evstatiev, M.; Schultz, J. M.; Fakirov, S.; Friedrich, K. *Polym. Eng. Sci.* **2001**, *41*, 192−204.
(9) Balijepalli, S.; Schultz, J. M.; Lin, J. S. *Macromolecules* **1996**, *29*, 6601−6611.
(10) Zener, C. *AIME Trans.* **1946**, *167*, 550.
(11) Jackson, K. A.; Hunt, J. D. *Trans. AIME* **1966**, *236*, 1129.
(12) Magnin, P.; Kurz, W. *Acta Metall.* **1987**, *35*, 1119.
(13) Trivedi, R.; Magnin, P. *Acta Metall. Mater.* **1991**, *39*, 453.
(14) Kurz, W.; Fischer, D. J. *Fundamentals of Solidification*; Trans Tech Publications: The Netherlands, 1992.
(15) Magnin, P.; Mason, J. T.; Trivedi, R. *Acta Metall. Mater.* **1991**, *39*, 469.
(16) Jincheng, L.; Elliott, R. *Acta Metall. Mater.* **1995**, *43*, 3301.
(17) Lauritzen, J. I.; Hoffman, J. D. *J. Res. Natl. Bur. Stand.* **1960**, *A64*, 73.
(18) Hoffman, J. D.; Lauritzen, J. I. *J. Res. Natl. Bur. Stand.* **1961**, *A65*, 297.
(19) Balijepalli, S.; Schultz, J. M. *Macromolecules* **1996**, *29*, 2095−2102.
(20) Kovacs, A. J.; Straupe, C.; Gonthier, A. J. *J. Polym. Sci., Polym. Symp.* **1977**, *59*, 31.
(21) Kramer, E. J.; Parker, R. L.; Palstrom, C. J. *Polymer* **1984**, *25*, 473.
(22) 2 Cheng, S. Z. D.; Barley, J. S.; von Meerwall, E. *J. Polym. Sci., Polym. Phys. Ed.* **1991**, *29*, 515.
(23) 3 Te Huieura, W. M.; Wang, R.; Callaghan, P. T. *Macromolecules* **1990**, *23*, 1658.
(24) Kit, K. M.; Schultz, J. M. *Macromolecules* **2002**, *35*, 9819−9824.

MA060097V